Video Article

Characterization of Surface Modifications by White Light Interferometry: Applications in Ion Sputtering, Laser Ablation, and Tribology Experiments

Sergey V. Baryshev[1], Robert A. Erck[2], Jerry F. Moore[3], Alexander V. Zinovev[1], C. Emil Tripa[1], Igor V. Veryovkin[1]

[1]Materials Science Division, Argonne National Laboratory

[2]Energy Systems Division, Argonne National Laboratory

[3]MassThink LLC

Correspondence to: Sergey V. Baryshev at sergey.v.baryshev@gmail.com, Robert A. Erck at erck@anl.gov

URL: http://www.jove.com/video/50260
DOI: doi:10.3791/50260

Keywords: Materials Science, Issue 72, Physics, Ion Beams (nuclear interactions), Light Reflection, Optical Properties, Semiconductor Materials, White Light Interferometry, Ion Sputtering, Laser Ablation, Femtosecond Lasers, Depth Profiling, Time-of-flight Mass Spectrometry, Tribology, Wear Analysis, Optical Profilometry, wear, friction, atomic force microscopy, AFM, scanning electron microscopy, SEM, imaging, visualization

Date Published: 2/27/2013

Citation: Baryshev, S.V., Erck, R.A., Moore, J.F., Zinovev, A.V., Tripa, C.E., Veryovkin, I.V. Characterization of Surface Modifications by White Light Interferometry: Applications in Ion Sputtering, Laser Ablation, and Tribology Experiments. *J. Vis. Exp.* (72), e50260, doi:10.3791/50260 (2013).

Abstract

In materials science and engineering it is often necessary to obtain quantitative measurements of surface topography with micrometer lateral resolution. From the measured surface, 3D topographic maps can be subsequently analyzed using a variety of software packages to extract the information that is needed.

In this article we describe how white light interferometry, and optical profilometry (OP) in general, combined with generic surface analysis software, can be used for materials science and engineering tasks. In this article, a number of applications of white light interferometry for investigation of surface modifications in mass spectrometry, and wear phenomena in tribology and lubrication are demonstrated. We characterize the products of the interaction of semiconductors and metals with energetic ions (sputtering), and laser irradiation (ablation), as well as *ex situ* measurements of wear of tribological test specimens.

Specifically, we will discuss:

i. Aspects of traditional ion sputtering-based mass spectrometry such as sputtering rates/yields measurements on Si and Cu and subsequent time-to-depth conversion.
ii. Results of quantitative characterization of the interaction of femtosecond laser irradiation with a semiconductor surface. These results are important for applications such as ablation mass spectrometry, where the quantities of evaporated material can be studied and controlled via pulse duration and energy per pulse. Thus, by determining the crater geometry one can define depth and lateral resolution versus experimental setup conditions.
iii. Measurements of surface roughness parameters in two dimensions, and quantitative measurements of the surface wear that occur as a result of friction and wear tests.

Some inherent drawbacks, possible artifacts, and uncertainty assessments of the white light interferometry approach will be discussed and explained.

Video Link

The video component of this article can be found at http://www.jove.com/video/50260/

Introduction

The surface of solid materials determines to a large extent properties of interest for those materials: electronically, structurally, and chemically. In many areas of research, the addition of material (for instance, thin film deposition by pulsed laser/magnetron sputtering deposition, physical/chemical vapor deposition), removal of material (reactive ion etching, ion sputtering, laser ablation, etc.), or some other processes, need to be characterized. Additionally, surface modification through interaction with energetic light pulses or charged particles has numerous applications and is of fundamental interest. Tribology, the study of friction and wear, is another area of interest. On a benchtop scale, a multitude of tribological test geometries exist. Non-conformal contact geometries may be used, and a ball or cylinder may be slid or rotated against a flat surface, another ball, or cylinder, for a length of time, and the amount of material that is removed is measured. Because the wear scar is three-dimensional and irregular in nature, optical profilometry may be the only technique suitable for obtaining accurate wear volume measurements. Common analysis tasks include also surface roughness parameters, step height, loss of material volume, trench depth, and so on; all of them can be obtained additionally to simple 2D and 3D topography visualization.

Optical profilometry refers to any optical method that is used to reconstruct the profile of surfaces. Profilometric methods include white light interferometric, laser, or confocal methods. Some optical profilometers obtain information through approaches based on conventional diffraction-limited microscope objectives. For example, a scanning laser may be integrated with a microscope to obtain topographic and true color information of surfaces. A second method uses a technique which exploits the extremely small depth of focus of conventional objectives to assemble a series of in-focus "image slices" of the surface to obtain a 3D topographic map.

In this work we show how a white light interferometric microscope/profilometer enables the measurement of the amount of material lost during mechanical wear processes, or during material etching processes such as ion sputtering craters or laser ablation. Most attention is paid to methodology of this method to illustrate its large installed capacity that makes it widely available and attractive for numerous applications. Most types of WLI employ the Mirau technique, which uses a mirror internal to the microscope objective to cause interference between a reference light signal and the light reflected from the sample surface. The choice of Mirau interferometry is dictated by simple convenience, because the entire Mirau interferometer can be fit inside the microscope objective lens and coupled to a regular optical microscope (**Figure 1**). A series of two-dimensional interferograms are acquired with a video camera, and software assembles a 3D topographic map. The white light source supplies broad spectrum illumination which helps to overcome the "fringe order" ambiguity inherent to a monochromatic source. A monochromatic source of light may be used to obtain more accurate measurement of shallow topographic features. The lateral resolution is fundamentally limited to $\lambda/2$ (numerical aperture, NA=1), but in most instances is larger, being determined by the NA of the objective, which is in turn connected to magnification/field-of-view size. **Table 1** in Ref. 1 has a direct comparison of all mentioned parameters. Depth resolution approaches ≈1 nm, being a function of the interferometric nature of the technique. Further information on Mirau WLI can be found in Refs. 2, 3. An introduction on white light interferometric approach can be found in Ref. 4.

Other methods for analysis of surfaces are atomic force microscopy (AFM), scanning electron microscopy (SEM), and stylus profilometry. The WLI technique compares favorably to these methods and has its own advantages and drawbacks that are due to the optical nature of the method.

The AFM is capable of obtaining 3D images and thus corresponding cross sections, but AFM has a limited scanning ability in the lateral (<100 μm) and depth (<10 μm) axes. In contrast to those, the main advantage of WLI is the flexible field-of-view (FOV) of up to a few millimeters with simultaneous real 3D imaging capability. In addition, as we will demonstrate it has wide vertical scanning range capacity, allowing one to solve a variety of problems of surface modification simply. Researchers who have worked with AFM are aware of the problem with plane positioning of a sample when measuring prolonged features of low vertical gradients. Generally, one may think of WLI/OP as an "express" technique over AFM. Of course, there are a number of areas for which only AFM is suitable: when lateral features to be resolved have characteristic dimensions smaller than the lateral resolution of WLI, or instances where data from WLI is ambiguous due to unknown or complex optical properties of a sample in a way that affects the accuracy of measurements (to be discussed later), etc.

The SEM is a powerful way to look at surfaces, being very flexible in terms of the FOV size with large depth of focus, larger than any conventional optical microscope can offer. At the same time, 3D imaging by SEM is cumbersome, particularly as it requires taking of stereo-pair images that then are converted to 3D images by the anaglyphic method, or through observing with optical viewers, or used for direct calculation of depths between different points of interest on a sample.[5] By contrast, WLI/OP profilometry offers easy-to-use 3D reconstruction with simultaneously flexible FOV. WLI scans through the full height range needed for the particular sample (from nanometers to hundreds of microns). WLI is unaffected by the electrical conductivity of the sample material, which may be a problem with SEM. WLI clearly does not require a vacuum. On the other hand there are a number of applications for which SEM provides superior information: lateral features to be resolved of characteristic dimensions below the lateral resolution of WLI, or cases where different parts of a sample can be topographically distinguished only when secondary electron emission coefficients differ.

One more technique for surface inspection, which is widely used in secondary ion mass spectrometry[6] and in the field of microelectromechanical systems characterization[7] is stylus profilometry. This technique is popular because of its simplicity and robustness. It is based on direct mechanical contact scanning of a stylus tip over the sample surface. This is a coarse contact tool, which is able to scan along a single line at a time. It makes 3D surface raster-scan imaging extremely time consuming. Another drawback of the stylus technique is the difficulty of measuring surface features of high aspect ratio and of size comparable with its characteristic tip size (submicron to several microns typically) that implies a tip radius and a tip apex angle. An advantage of stylus profilometry is its insensitivity to varying optical properties of a sample, which can affect the accuracy of WLI/OP measurements (to be discussed later).

The surface maps in the present article were obtained using a conventional Mirau-type WLI (**Figure 1**). Many companies such as Zygo, KLA-Tencor, nanoScience, Zemetrics, Nanovea, FRT, Keyence, Bruker, and Taylor Hobson produce commercial table-top OP instruments. The acquired maps were reconstructed and processed using commercial software of the type that is commonly used for WLI, scanning electron, or probe microscopy. The software has the ability to perform mathematical manipulations of the surface, cross section profile analysis, void and material volume calculations, and plane correction. Other software packages may automate some of these features.

Protocol

1. Hardware Alignment for General WLI Scan

To obtain quantitative information through WLI, the following steps may serve as a guideline. It is assumed that the operator has basic knowledge of interferometer operation. The guidelines are common regardless of the specific instrument. For some investigations, the specimen will be flat. For others, the specimen may be curved.

1. Place the sample on the stage with the feature (ion sputtered crater, ion beam/ablated spot, or wear scar) facing straight up. Use a low-magnification objective and focus the instrument on it. For best resolution obtain an image in which the object of interest largely fills the screen, see **Figure 2** for an example of a ball.

2. Adjust the vertical position of the specimen so that interference fringes appear near the feature of interest. For a flat surface it is desirable that the specimen is tilted such that the plane is perpendicular to the optical axis, *i.e.* the fringe spacing will be large. For a curved surface (*e.g.* a ball), the specimen should be oriented such that fringes are centrally located around the feature, such as in **Figure 3**.
3. Obtain a scan according to the instrument instructions. It may be necessary to adjust the illumination or scan height in order to obtain the best topographic map. Fill in any bad or missing data using the interpolate function, and then save the topographic map.

2. Volume Analysis Using Generic Software

In tribology, testing machines often employ non-conformal contact testing geometries such as a ball or a cylinder that is slid or rotated against a flat or another cylinder. Typically, material is lost at the point of sliding contact, although sometimes material may transfer from one surface to another, and this "transfer layer" will be measured as a surplus of material on one of the contacting specimens. Because the wear scar is three-dimensional and irregular in nature, optical profilometry may be the only technique suitable for obtaining accurate wear volume measurements - approximations are not valid. The goal is to measure the very small amounts of material which may be lost (or gained) in the contacting region at the completion of a test.

The basic principle of measurement is to define a mathematical plane at the level of the undisturbed surface: surface analysis software assumes that there is a "solid surface" (zero level), whatever above this level is "empty." The analysis function that measures the integrated removed volume below the plane of the "solid surface" will be referred to as "void volume." The function that measures the integrated volume above the plane of the "solid surface" (*e.g.* an accumulation of debris) will be called the "material volume."

Real undisturbed surfaces are seldom perfectly smooth and flat. For greatest accuracy in measuring small features it is good practice to define an area of interest (AOI); the area outside of which is excluded from analysis. The AOI is used to restrict the measurement area because irregularities in the surface contribute additional volume to the calculations that is not truly from the disturbed area.

3. Flat Surface - Mechanical Wear Analysis

1. Volume analysis of a flat surface with a trench scar or depression, whether generated by mechanical wear, ion beam sputtering, or laser ablation, is easy to perform. Obtain an image such as **Figure 4** left which shows a mechanical scar on a polished steel surface. Select an AOI that excludes the depression and then use whatever tilt and/or curvature removal function is available to level the undisturbed surface to maximum flatness. Then use the software to set the average surface height to Z=0. **Figure 4** right is a pseudocolor view of a scar on a flat surface after these steps. In this view the excluded "void volume" is tinted red. In this color scheme, the dark brown denotes low areas, while orange denotes high areas.
2. Delete the AOI. If the software has an automated volume measuring function, place a region of measurement over the scar. In this software, the measuring function will tally the "void and material volume" shown with blue tint in **Figure 5**. Total wear is "material volume" above the plane subtracted from "void volume." This is the volume change of the disturbed surface. (For software that does not have this function, but does have a histogram, or to clearly visualize which areas are raised above the surface or are below the surface, skip step 3.2 and go to step 3.3.)

The following three steps describe an alternate method of measuring wear volume.

3. Invert the AOI from step 3.1 to enable the scar region to be analyzed (the scar is included now).
4. Generate a histogram of the data. The histogram is a graph of vertical height on the abscissa vs. the frequency of occurrence on the ordinate. Place one cursor at the Z=0 position (**Figure 6** left). This may not be at the peak of the histogram. In this figure the cursors have been set up to selectively analyze only the missing material below the plane. The software integrates the total volume between the two cursors. The red tinted area shows what is omitted. The orange untinted areas in **Figure 6** right are below the surface. The histogram function should generate a "void volume" number with the cursors positioned as shown to measure the material lost from the surface.
5. Using the same histogram, place the other cursor this time at the Z=0 height position (**Figure 7** left), and the other at the opposite end. The orange untinted areas in **Figure 7** right are above the surface. The histogram function should generate a "material volume" number, *i.e.* surplus material raised above the flat surface. Total wear is "material volume" subtracted from "void volume," the same as in step 3.2. The histogram method should give the same wear volume as in step 3.2, but it provides additional details about the distribution of raised and lowered material, and shows a map of the distribution of this area.

In the example above there is no net material lost from the wear scar, instead there is material gain. This is unusual, but sometimes occurs when material transfers from one test counterface to another.

The same "flat surface characterization" approaches are beneficial for obtaining volumes removed in experiments with ion sputtering and laser ablation, considered in examples that follow.

4. Flat Surface - Craters and Ion Beam Profiles Measurements to Estimate Sputtering Yield, and to Perform Time-to-depth Calibration

As an alternative to the known and widely employed method for estimating sputtering yields using mass-loss method, based on direct weighing or quartz microcrystal balance,[8, 9] we find that the WLI method is useful for direct visualization of the sputtered ion beam spots/craters obtained by static sputtering/raster scanning of an ion beam. **Figure 8** compares longitudinal cross sections of a spot (green solid and blue dotted lines) of a normally incident static 5 keV and 150 eV Ar^+ ion beams against their craters (olive open circles and cyan open diamonds) obtained by

100×100 pixels digital raster scanning of the same ion beam over the surface of a Cu(110) single crystal. The curve corresponding to the static beam overlaps one edge of the crater to demonstrate how raster scan of the ion beam generates the crater during sputter depth profiling.

5. Flat Surface - Characterization of Ultrafast Laser Ablation

Ultrafast laser ablation is recognized as a method for removing material from a solid while minimizing the heat affected zone.[10] This process enables high rate micromachining with high aspect ratios and minimal damage (cracking, oxidation) to the remaining material, and opens up the possibility of efficient ablation of transparent materials.[11] More recently, interest has developed in using ultrafast ablation as an analytical tool.[12-15] The high nonlinearity of the ablation process also provides a means of reducing the ablated spot size significantly below the irradiated spot size (as typically defined by $1/e^2$) and even below the diffraction limit, as has been demonstrated.[16] Depth resolution, while not competitive with the best ion beam methods, may be <20 nm. Removal rates can easily be increased nonlinearly by increasing the laser fluence, so that very rapid profiling through microns of material is possible. Ideally, characterizing material removal by ultrafast ablation requires a technique that is fast and quantitative and well calibrated, all characteristics fulfilled by WLI.

Figure 9 shows pseudocolor images of two neighboring craters formed by repetitive ablation of GaAs with an ultrafast (60 fs, 800 nm) laser beam focused to a spot size of ≈8 μm and having fluences corresponding to 0.4 and 1.0 J/cm^2.

6. Curved Surfaces - Mechanical Wear Analysis

Volume analysis of a curved regular surface (ball or cylinder) is similar to that of a flat, but requires curvature removal. The following protocol shows an analysis of a circular wear scar on a steel ball. To find the volume lost from a ball it is necessary to do mathematical processing to transform a ball with a flat area into a flat plane with an indentation, then measure the volume of the indentation as was done in Section 3 on flat surfaces. A wear scar on a ball will be measured, first using the simpler automatic technique, then with the histogram technique.

1. **Figure 10** left shows an isometric view of a wear scar on a ball. Select an AOI that excludes the wear scar, and select the software curve fitting tool that will transform the surface so that it is a worn depression in the middle of an undisturbed flat area. Because curvature removal may be an iterative technique it may be necessary to run the fit several times so that the undisturbed area is flat to nm level accuracy. Any visible non-uniformity outside of the wear scar indicates a problem and the calculation will not be correct. Set the average height outside the scar to Z=0. **Figure 10** right shows a pseudocolor view of the scar after curvature removal and setting Z=0 with an AOI properly masking the worn area.
2. Use the measuring tool, if available, to analyze the wear, as shown in **Figure 11**. Total wear volume is "material volume" subtracted from the "void volume."

The following steps describe an alternate method of measuring wear volume.

3. In the same manner as step 3.3, invert the AOI so that the wear scar is included. Generate a histogram of the data. Place one cursor at the Z=0 position (**Figure 12** left). The orange untinted areas in **Figure 12** right are below the surface. The histogram function should generate a "void volume" number.
4. Using the same histogram, place the other cursor this time at the Z=0 height position (**Figure 13** left), and the other at the opposite end. The orange untinted areas in **Figure 13** right are above the surface. The histogram function should generate a "material volume" number. Total wear volume is "material volume" above the plane subtracted from "void volume," the same as in step 3.2. The histogram method should calculate the same wear volume as in step 6.2, but it provides additional details about the distribution of raised and lowered material, and shows a map of the distribution of this area.

Representative Results

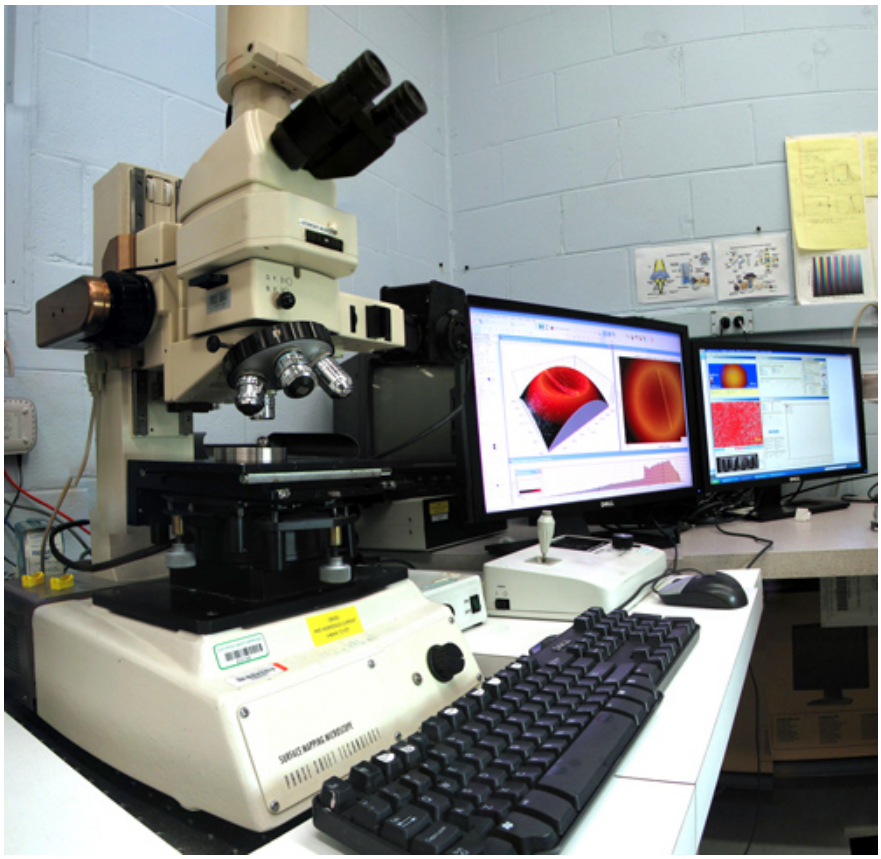

Figure 1. Photograph of a simple profilometer used in the present study: a multiple objective turret is seen in the picture. Two objectives are standard (10x and 50x), and two are Mirau objectives (10x and 50x). This microscope has an intermediate magnification feature that enables step-wise magnification multipliers of 0.62, 1.00, 1.25, or 2.00 to be selected. Click here to view larger figure.

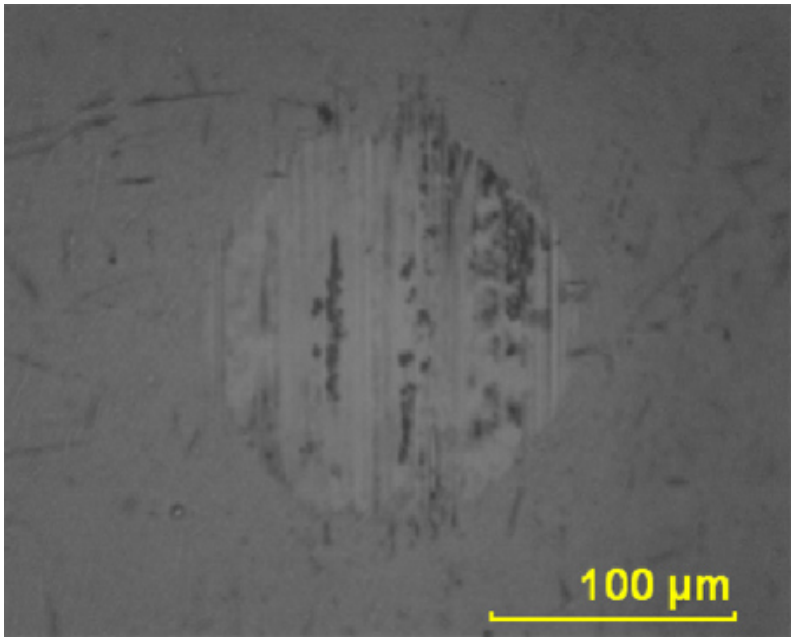

Figure 2. Normal appearance of wear scar on steel ball. Click here to view larger figure.

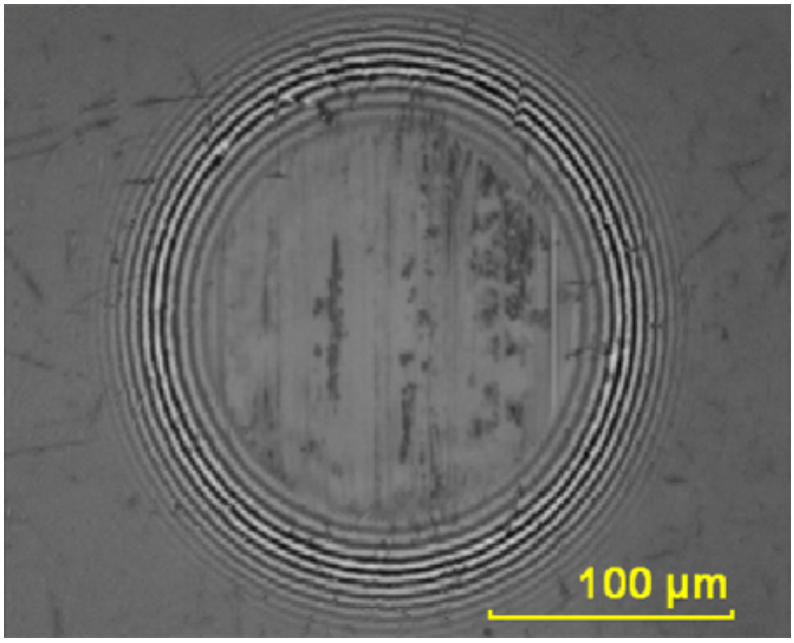

Figure 3. Interference fringes centrally located around wear scar. Click here to view larger figure.

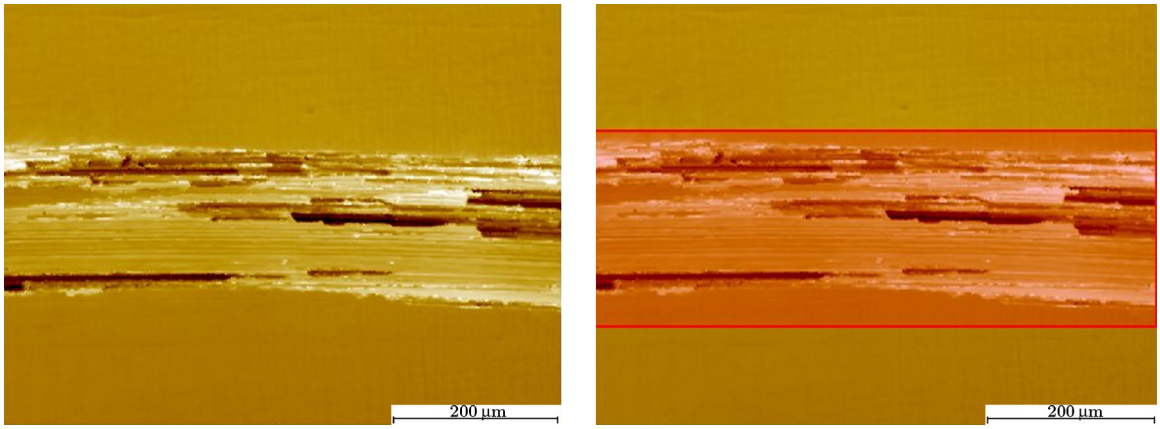

Figure 4. Left: Pseudocolor view of a scar on a flat surface. **Right:** AOI denoted in red, after leveling. Click here to view larger figure.

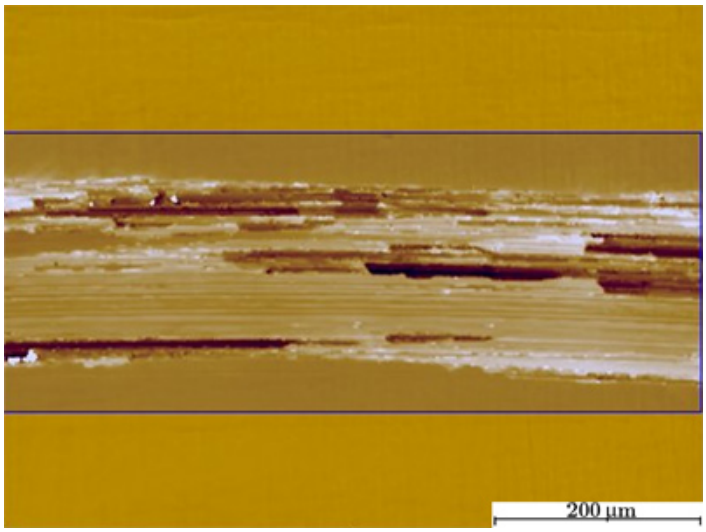

Figure 5. Image showing tally region of measuring tool. Click here to view larger figure.

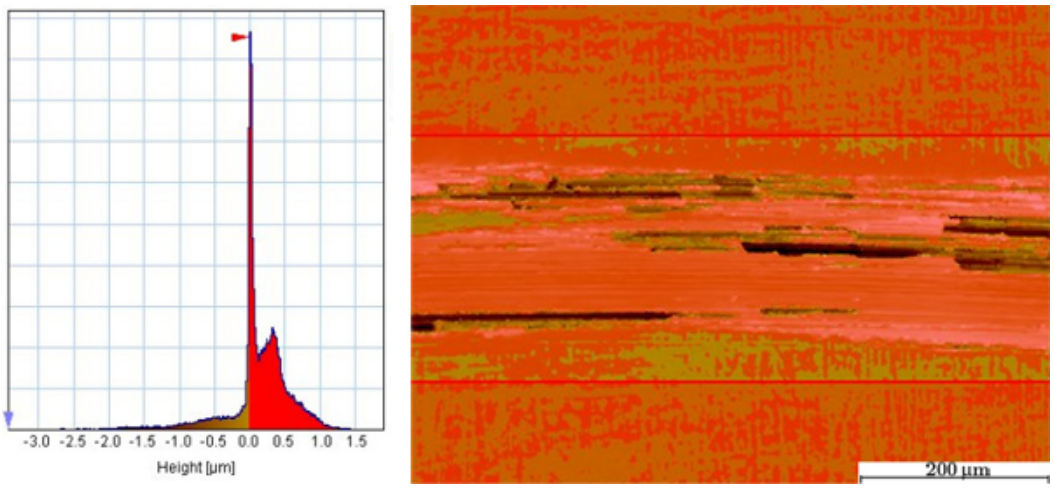

Figure 6. Left: Histogram of wear scar with cursors adjusted to measure "void volume." **Right:** Pseudocolor image. Click here to view larger figure.

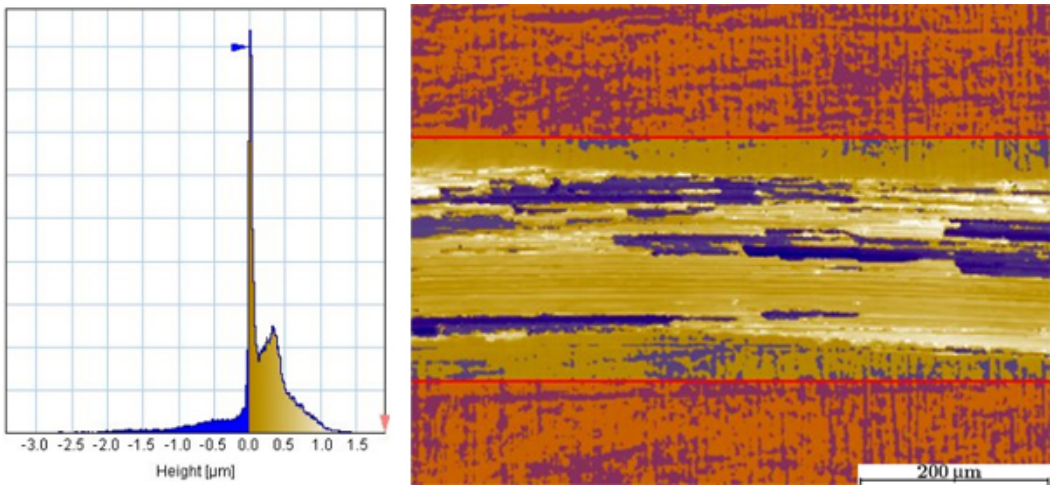

Figure 7. Left: Histogram of wear scar with cursors adjusted to measure "material volume." **Right:** Pseudocolor image. Click here to view larger figure.

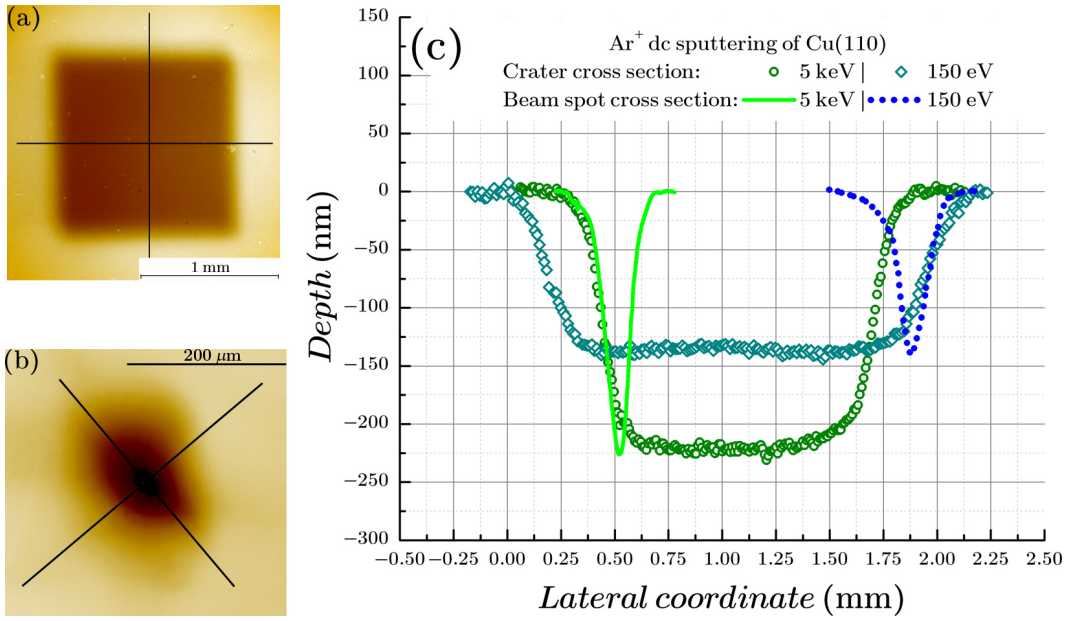

Figure 8. (a) and **(b)** Pseudocolor 2D top view of sputtered crater and spot, respectively. Black lines are directions along which cross sections plotted in **(c)** were measured, horizontal line is $X_{profile}$, vertical is $Y_{profile}$, **(c)** Beam spot and crater cross sections superimposed. Measurements were made on Cu(110) sputtered by normally incident Ar^+ ion beam with 5 keV (olive open circles and green solid line) and 150 eV (cyan open diamonds and blue dotted line) energies. Click here to view larger figure.

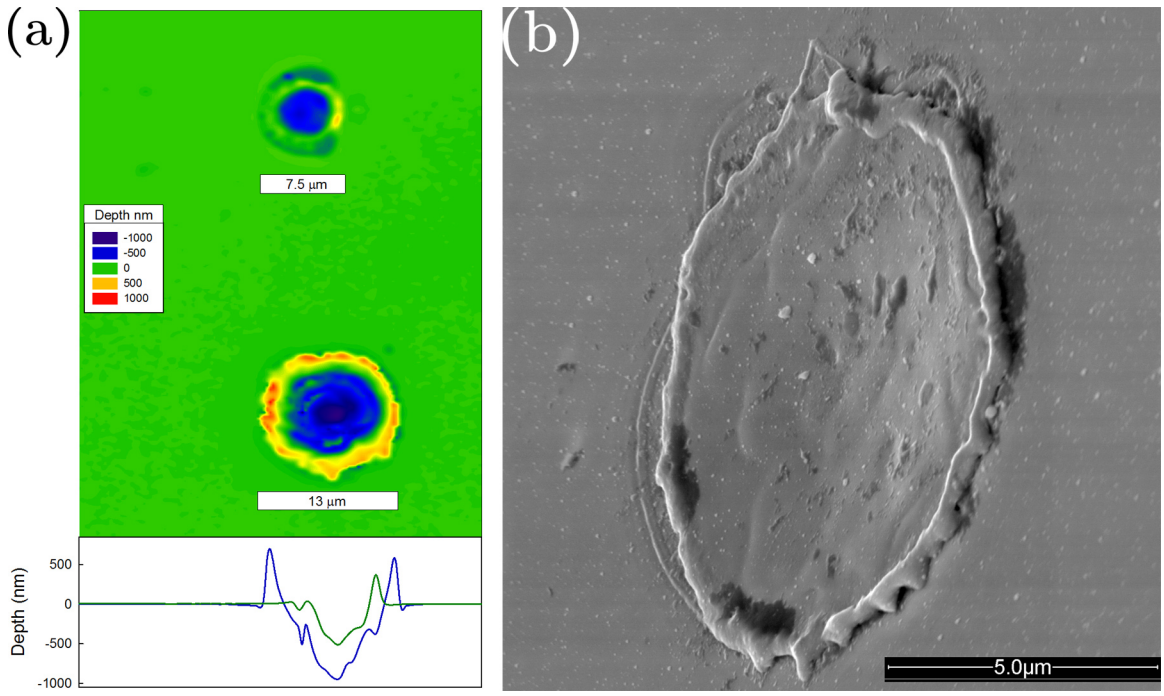

Figure 9. **(a)** Pseudocolor 2D top views of craters produced with low fluence (top) and high fluence (bottom) 800 nm irradiation of GaAs for ≈100 shots at 1 kHz repetition rate and a pulse width of 60 fsec. The scale bars indicate hole diameters, measured to the outer edge of the diffraction ring. Focal position and spot size are the same, indicating that the ablated crater size and depth depends strongly on the fluence. Plot at figure bottom shows cross section of each hole, with centroids adjusted to overlap; **(b)** SEM image of the larger crater captured at 60 degrees sample tilt to reveal if peaking outer ring (yellow in WLI picture) is real. Click here to view larger figure.

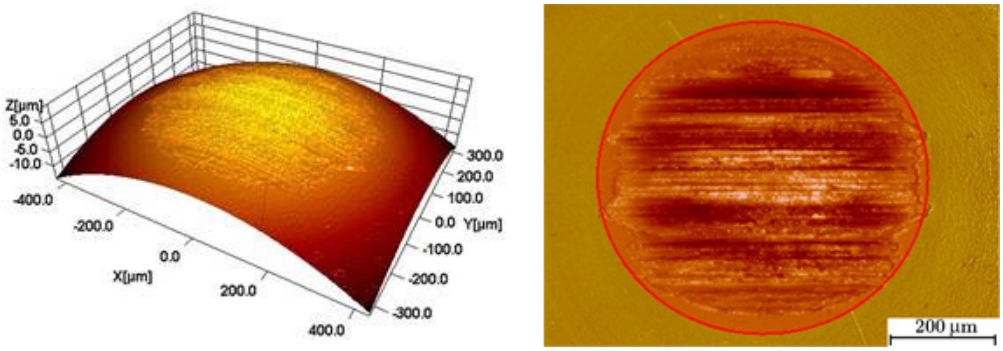

Figure 10. **Left:** Isometric view of wear scar with transfer film. **Right:** Proper AOI on ball excluding wear scar after curvature removal and Z=0.

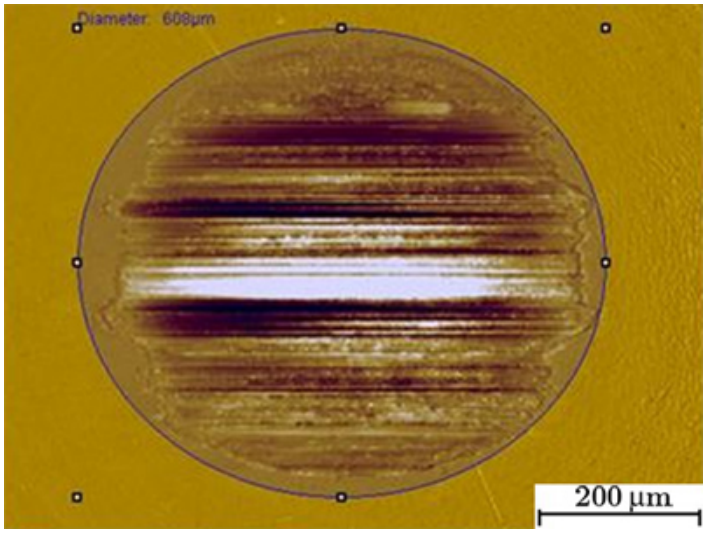

Figure 11. Pseudocolor view of wear scar with measuring tool. Click here to view larger figure.

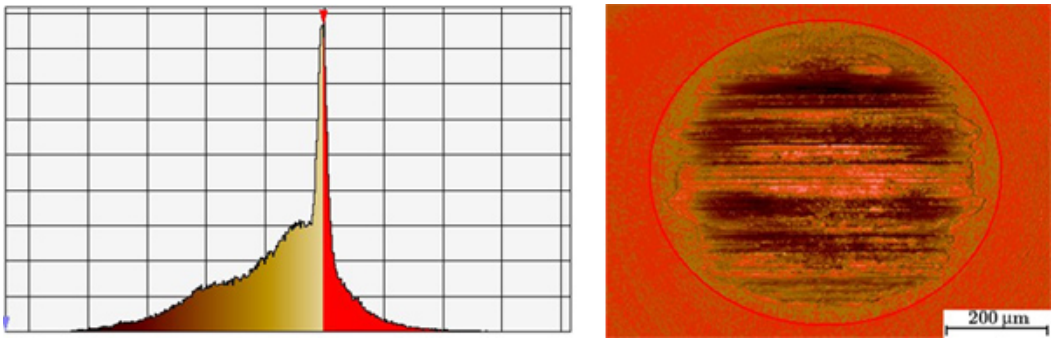

Figure 12. Left: Histogram of wear scar with cursors adjusted to measure "void volume." **Right:** Pseudocolor image. Click here to view larger figure.

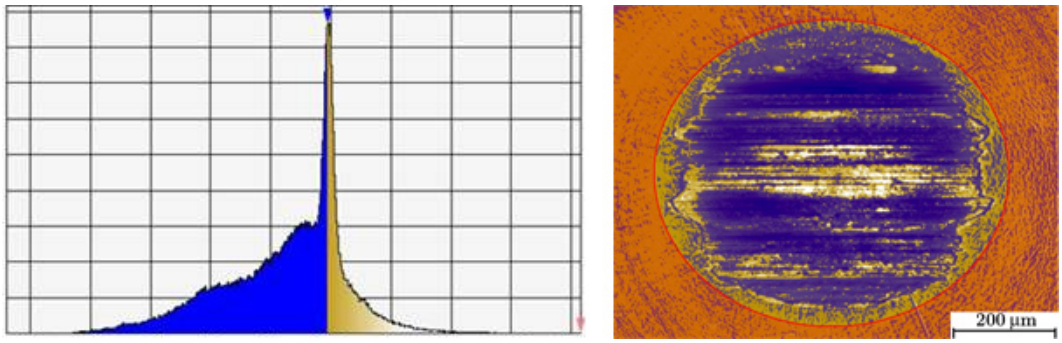

Figure 13. Left: Histogram of wear scar with cursors adjusted to measure "material volume." **Right:** Pseudocolor image.

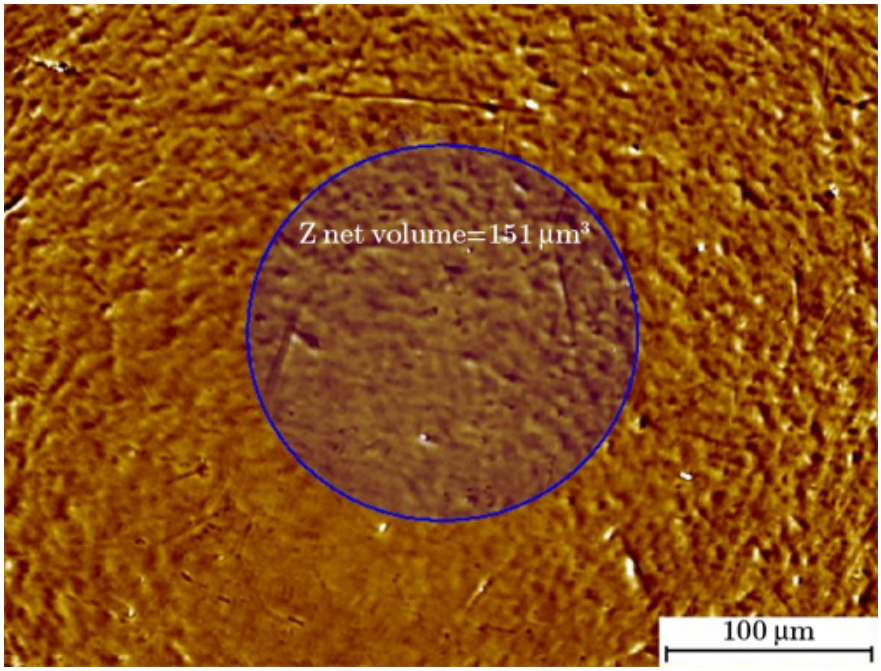

Figure 14. An example of an analysis performed on a pristine ball sample to estimate uncertainty in measurement. Click here to view larger figure.

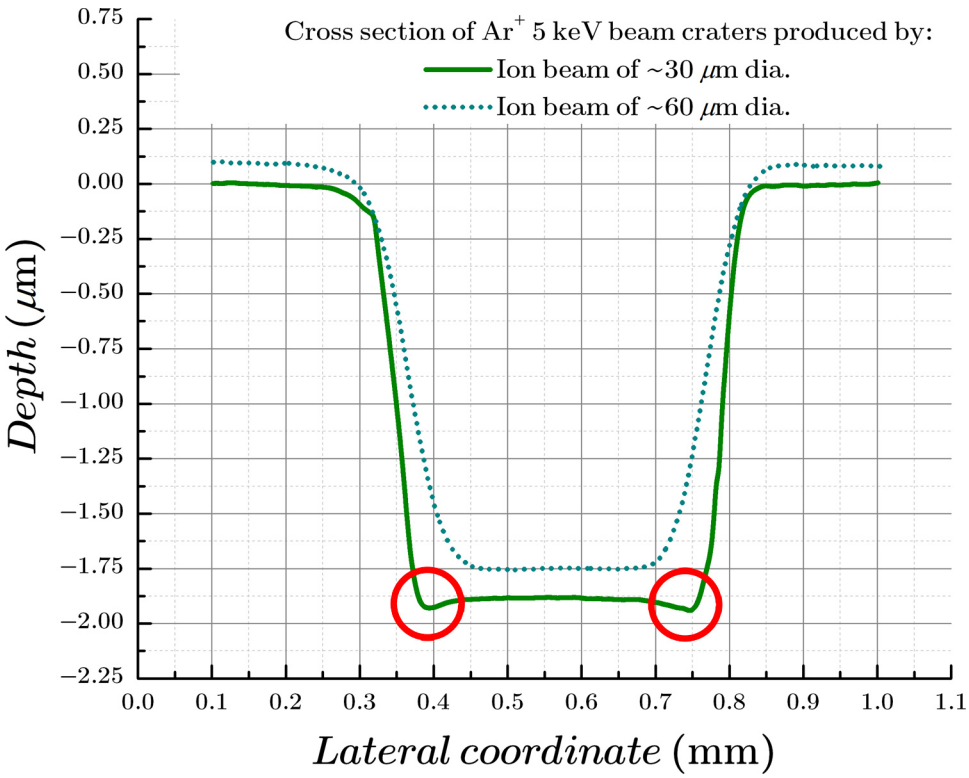

Figure 15. Solid line is a cross section of a crater in Si(100) with very sharp edges produced by raster scanned tightly focused 5 keV ion beam of ≈30 μm in diameter, while dotted one is a crater obtained through the same procedure at less focused beam of ≈60 μm in diameter. Red circles at the bottom show areas of batwings. Click here to view larger figure.

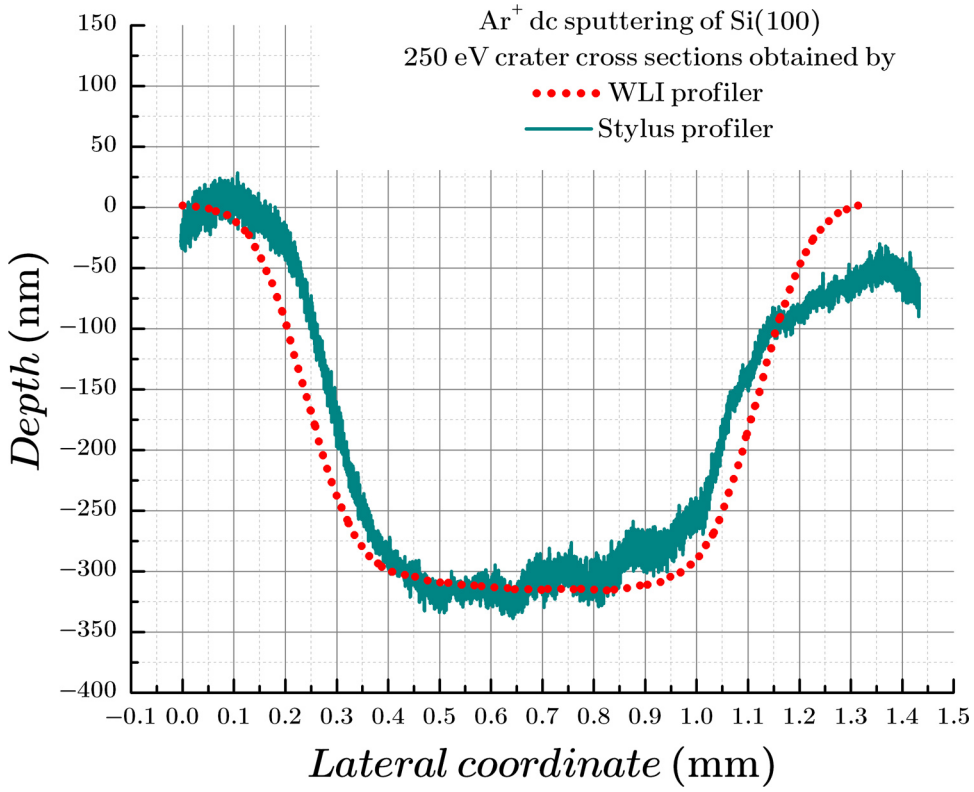

Figure 16. Direct comparison of the same ion sputtered crater in Si(100) probed by WLI and stylus profilers in order to independently prove a correct depth calibration of WLI. Click here to view larger figure.

Discussion

Example 1

WLI is not widely used for surface characterization in tribological work, but it is in fact a powerful method for quantitative measurement of wear volumes for many contact geometries. WLI produces a full 3D representation of the surface that can be analyzed using any of several visualization software packages. These packages enable various types of measurements to be performed. For greater lateral resolution, images can be "stitched" together to produce wide-area information (several mm), with µm resolution.

For non-tribological work, WLI can be used to measure surface features which are difficult to measure using AFM or other contact means. Fu *et al.* studied the effect of Ga ion beam parameters on the micromachining of Si surfaces. AFM was used to measure the surface profile, but the results were limited due to the restricted vertical range of the AFM cantilever tip, and damage caused by the tip for large pit depths. Instead, the workers found WLI to be more useful for measuring large depths while preserving features and being able to easily measure vertical sidewalls.[17]

In tribology, analysis software can extract statistical surface roughness parameters of worn surfaces, which can be compared with analytical models of surface topography generated by tribological processes, *e.g.* machining. Jiang *et al.* used this capability to study surface roughness as a function of milling parameters and compare with analytical models.[18]

A very simple use of WLI is for measuring the material loss from a wear scar during unidirectional sliding of a pin on a flat disk. Reiter *et al.* used WLI to scan wear tracks and calculate the wear volumes and hence wear rates for a series of ball on disk tests. Because the 2D surface is reconstructed, it is a simple matter to determine the depth and breadth of a wear scar, and thus calculate wear volume. In this sense, WLI serves as nothing more than an enhanced stylus profilometer.[19]

More powerfully, WLI can be used to measure the volume of wear lost by a sliding contact if the profile of the original surface is known. In the simplest example, a groove or crater is worn into a flat surface. The wear volume is simply the volume of material that is removed from the flat surface. Surface analysis programs enable the volumetric deviation from a flat surface, *i.e.* the volume lost, to be measured. These measurements are easiest when the original counterface is a symmetrical surface: flat, spherical, or cylindrical. Devillez *et al.* sketches out a method by which WLI was used to measure the volume lost from the surface of a cutting tool. The local area of the flank was initially flat, and it was relatively simple to calculate the difference between the original surface and the wear groove that was produced on the surface.[20] When the surface is not flat, then an additional step in the procedure is necessary in order to measure wear volume. If the original surface is geometrically regular, then it is possible to mathematically remove the curvature of the surface so that a flat plane is produced, while simultaneously deforming the wear scar in the same manner. The deviation from the plane can easily be calculated.

In biomedical tribology, WLI, sometimes called vertical scanning interferometry in the medical literature, can be used to measure the surfaces of native and worn articular cartilage. Topographic information can be obtained, but the technique is hindered by the fact that the surface of live cartilage is dynamic and moves as water is lost or absorbed.[21]

With this example we tried to show how WLI can be used for routine analysis in tribology; additional background can be found in Refs. 22, 23, and some references therein.

Example 2

In many experiments designed to determine sputtering yields (SY) of various materials under specific ion bombardment conditions, uncertainties in ion beam parameters can propagate and result in uncertain sputtering yield values.[24] For example, it can be challenging to determine shapes of ion beam profiles and the corresponding operational current densities, especially when the projectile energy goes below 1 keV and then further approaches the sputtering threshold. Moreover, under such conditions, the focusing of the ion beam is in question, and the relative spread $\Delta\varepsilon/\varepsilon$ in the initial kinetic energy distribution of ions[25] can have strong influence on experimental results.[9, 26]

By combining the WLI visualization with precise measurements of the total ion current by a Faraday cup (FC), the SY and the operating current density can be obtained simultaneously. Besides, this approach appears to be very helpful in estimating the extent of undesirable "wings" of the ion beam profile to help in aligning ion beam sources. The sputtering yield Y is then estimated by the following expression

$$Y = \frac{\rho \cdot V \cdot e}{I \cdot \tau \cdot M_{atom}}$$

where I, direct current of an ion beam; τ, time of sputtering; M_{atom}, mass of a matrix atom in grams; ρ, density; e, the elementary charge. V is the volume of the removed sample material obtained by means of the WLI measurement. Volume calculations can be performed either by using both approaches described in the Protocol for flat surfaces, depending on a type of post-processing software available, or by three dimensional integration based on cross sections in two orthogonal directions centered on the eroded surface area (black lines in **Figure 8a** and **8b**) simply by

$$V = X_{profile}\,Area \times \frac{Y_{profile}\,Area}{\left|Max - Min\right|_{Y_{profile}}} =$$

$$= \sum_i (X^{i+1}_{lateral} - X^{i}_{lateral}) \cdot \frac{(X^{i+1}_{depth} - X^{i}_{depth})}{2} \times (Y^{i+1}_{lateral} - Y^{i}_{lateral}) \cdot \frac{(Y^{i+1}_{depth} - Y^{i}_{depth})}{\left|Max - Min\right|_{Y_{profile}}}$$

in the event that one has no option to perform detailed post-processing as described in the Protocol. The $|Max\text{-}Min|_{Yprofile}$ parameter in the second multiplier term is used not to take the crater depth into account two different times, when calculating the V.

The ion beam currents are measured *in situ* by a custom graphite FC consisting of an internal pin (inlet holes of 250 μm dia.) and the external surface. This design provides coarse control over the ion beam focusing conditions by measuring "internal" and "external" (mostly attributed to "wings") components of the delivered current. Position of the FC fully simulates a sample surface positioning with respect to focusing and directing ion optics of our mass spectrometer.[27] The measurement of energy spread Δε of the low energy system[27] can be accomplished using the same FC. In this case, FC can be externally biased by a voltage 0 to 5 kV, and the total current as a function of suppression voltage is measured. In such a manner, the inherent Δε was estimated to be 23 eV.

The symmetric profile that is seen in **Figure 8** suggests that there is good alignment of the ion beam column, and FWHM of 120 μm at a total current of 2 μA. The WLI approach allows one to characterize the ion sputtering with the identical normally incident ion beam decelerated to 150 eV by the target potential. In this case, the cross section of the static beam spot is shown by a blue dotted line, and the crater cross section is shown by cyan open diamonds. The ion column enabled delivery of the same 2 μA of Ar^+ current on the target because the deceleration of the beam from the nominal 5 keV energy to 150 eV occurred in the immediate vicinity of the target, and in such a way that its optimal focusing was maintained by an electrostatic lens (the FWHM of 150 μm in **Figure 8c** is evidence of that).[27] The sputtered crater has in this case a larger lateral size because the deflection voltages of the raster-generating octupole were kept unchanged for the two primary ion impact energies, resulting in additional beam swinging due to the target potential.

Based on the WLI data, sputtering yields of Cu(110) at 5 keV and 150 eV ion impact energies were determined. An obtained SY value of 1.8 at/ion for the former case was in good agreement with literature data.[28] For the latter one, the sputtering yield was 0.2 at/ion (rare or lack in the literature).

For SY estimates, our results demonstrate an alternative experimental approach, which can also be used to verify experimental data and to "tweak" adjustable parameters of predictive models[29, 30] and calculation codes such as SRIM[31] and TRIDYN,[32] as well as to generate reference data for many technological applications.[6, 9, 33-36] In addition, this approach is capable of accurate quantifying sputtering rates for organic materials and solids under bombardment with a variety of primary species, commonly used atomic ions and relatively new molecular and cluster ions, such as in Refs. 37, 38. Thus it helps to resolve a problem of time (or primary ion fluence) to depth conversion in depth profiling

experiments by using an average parameter called the sputtering rate $S_z = \frac{d}{\tau}$ where d is a total depth measured by WLI and τ, as mentioned above, total time of sputtering.

Example 3

As in the case with ion beam sputtering, the ablation yield is an important parameter for analytical applications. For ablation, this value is usually expressed in terms of removal rate per shot, or alternatively removal rate per unit of time with a given laser repetition rate. Because there is minimal thermal loading of materials, repetition rates may be very high (MHz) and is often limited by the rate at which the beam can be moved over the material. Additionally, there are multiple material ablation thresholds, corresponding to different fundamental ablation mechanisms.[39] The predominant analytical tools using ultrafast laser ablation require high fluences (>5 J/cm^2) and correspondingly high removal rates and consume relatively large quantities of sample for analysis.[40, 41]

In principle the ions formed during the ablation process can be analyzed directly, or ablated neutrals can be ionized with a second laser, leading to a more sensitive and higher spatial resolution technique. As is seen in **Figure 9a**, two craters ablated under identical conditions, with the exception of fluence, will have dramatically different shapes. These craters are representative of a larger set of craters formed on a polished single crystal GaAs sample. By simply decreasing the fluence from 1 J/cm^2 to 0.4 J/cm^2 (the latter value being about twice the ablation threshold for GaAs),[42] the crater diameter is reduced by nearly half, and the average removal rate at the center of the crater is reduced from about 10 nm/shot to 5 nm/shot. The mass removal rate is apparently reduced by a factor of six, improving the corresponding analytical volume resolution.

It is important to note that the pronounced ring structure observed around each hole (**Figure 9a**) should be interpreted with care, since it may be due to scattering of the light from the interferometer. Although it is possible to get ring-shaped crater material ejecta, they are generally only seen with much longer pulsed lasers.[27] This optical artifact can be expected if the radius of the crater's edge is near, or below the diffraction limit for the average wavelength in the far field conditions of the microscope (roughly 1 μm in this case). In such situations, if measurement of the crater wall radius is crucial a complimentary technique such as those described above should be employed - see the following section on artifacts and limitations of WLI. However, if the main goal is to measure the crater depth, with a secondary goal to ensure that a threshold radius near the diffraction limit is not exceeded, then WLI is well suited for quickly measuring large numbers of craters.

Some typical artifacts/errors and limitations of WLI

1. Error estimation and uncertainty assessment

All real surfaces are rough and irregular to some extent, and no measurement technique is perfect. These imperfections will introduce uncertainties in the measurement of material loss. There are three sources of error. First, there is measurement error and noise inherent in the profilometer. Second, errors may arise due to imperfect curvature removal if this step is performed. Third, the original undamaged surface may be rough and irregular, which can lead to subtraction errors because the original surface is not known to perfect accuracy. An estimate of the magnitude of the total error can be obtained by simply performing several measurements on pristine sample surfaces using the identical processing/levelling technique as done on a modified sample surface. **Figure 14** shows one of five measurements made of pristine ball surfaces. The resulting average volume was 92 μm^3 with a standard deviation of 184 μm^3, instead of the expected value of zero. This indicates that for these samples and specific processing technique used, there is statistical variation of 184 μm^3 and a systematic error of 92 μm^3.

Also, let us briefly describe typical artifacts and limitations one meets when using WLI approach. These artifacts contribute additional uncertainties which affect precision of final results. For each specific WLI application instance, they should be addressed separately.

2. A single or multilayer constituent film of optical properties that differ from those of a base/substrate. Transparent/semitransparent film on a reflective base

The simplest type of WLI requires optical specular reflection from a surface. If the entire surface has the same reflectivity in terms of phase change of the reflected wave, then a measurement accurate to nm will be obtained. For inhomogenous samples (for instance, integrated circuit patterns), a correction needs to be applied based on the nature of the particular material. This effect is addressed in a paper by Harasaki *et al.* [43] Offsets as large as 36 nm may occur for Ag/Au pairs. In such cases, detection part of WLI can be easily "confused" by different optical responses in terms of phase shifts in a way that gives a wrong estimation of the full depth. It is also common, if one sees that a bowl is inverted into a pedestal that sticks above the zero level of a pristine surface; the height is skewed as well. This effect is nicely demonstrated in **Figure 13** in Ref. 7. A straightforward way to avoid such problems is to uniformly cover the entire surface with some known reflective material so it will have the same optical response to a WLI detector. Then this measurement problem disappears. In Ref. 7, this problem was resolved through covering of a layered system, SiO_2 on top of Ti base, with gold film. At the same time, it is worth mentioning that in some cases one might try to deal with optically transparent layers. The basis of such a measurement by WLI is somewhat different and has to do with the limited coherence length of natural (white) light. It was demonstrated that transparent films of ≈10 nm and higher thickness on a reflective substrate can be measured by WLI. A good description of this procedure can be found in Refs. 44 and 45.

3. Batwings

As mentioned with respect to what is shown in **Figure 9** above, sharp features such as steps and crater edges may cause diffraction of the light from the interferometer, leading to anomalous signals known as "batwings."[46] In general, this occurs when the lateral dimensions of such features are near the diffraction limit and the step height is below the coherence length of the light. Experimental approaches have been developed to minimize such artifacts (see for example Ref. 47). **Figure 15** demonstrates this effect in case of ion sputtering experiments. The green solid line is a crater produced by a "sharply" focused Ar^+ ion beam of ≈30 μm dia. that gave abrupt change in heights between the surface

and the crater's bottom with vertical walls. On the one hand, it suggests a very good ion beam alignment, but at the same time those artifacts called "batwings" are introduced by WLI into the final profiles reconstruction, and so should be excluded from volume removed calculations. There is a dotted cyan line in the same plot, which represents exactly the same sputtering conditions but under the ≈60 μm dia. beam. As one can clearly see, "batwings" completely disappeared. This is due to pronounced change in transition gradient as the focusing condition differs.

Concluding Remarks

It is important to keep in mind if a research work connected with a new type of sample is started using WLI it is always a good idea to establish whether or not WLI is suitable for those purposes. If yes, then it is necessary to calibrate/check calibration using an independent approach; and only after that WLI becomes an express method of getting bulk amounts of results. There are three of them as was already mentioned: AFM, SEM and stylus. **Figures 9b** and **16** are examples of comparing of WLI results to SEM and stylus, respectively.

Figure 9b answers a question if the outer ring spikes of ejected material of larger ablated craters seen in WLI pictures are real. It is hard to determine precisely, but results of performed SEM imaging compare favorably with what WLI provides in terms of height of sharp ring structure observed around each hole ≈400 nm (≈500 nm from WLI profile) and ≈12 μm dia. (≈13 average dia. deduced from WLI profiles).

Figure 16 is an example of how WLI profiling results can be confirmed by stylus profiler, if dimensions of modified area are suitable for this purpose. The idea behind this experiment was to check depth calibration through an independent technique. The object is a crater obtained by Ar^+ 5 keV ions in Si substrate, the lateral dimensions, lying beyond AFM capabilities, are such that use of stylus is favored. In **Figure 16** two profiles obtained through WLI and stylus superimposed one onto another. Direct comparison of the data suggested that results obtained by WLI in terms of depth are correct. The lateral dimension is also reproducible with an only exception: laterally crater measured by stylus looks narrower against WLI. Taking that the sample is single-component and all the transition spatial gradients are small, it is reasonable to assume that WLI data reflect actual size of the removed area, and smaller size in stylus representation is due to convolution of the real crater size with characteristic probing tip size. As a rule, depth calibration of our WLI profilometer is accomplished through Ted Pella AFM step-like standard of 500 nm height.

Disclosures

No conflicts of interest declared.

Acknowledgements

The irradiated GaAs sample was provided by Yang Cui of the University of Illinois at Chicago. This work was supported under Contract No. DE-AC02-06CH11357 between UChicago Argonne, LLC and the U.S. Department of Energy and by NASA through grants NNH08AH761 and NNH08ZDA001N, and the Office of Vehicle Technologies of the U.S. Department of Energy under contract DE-AC02-06CH11357. The electron microscopy was accomplished at the Electron Microscopy Center for Materials Research at Argonne National Laboratory, a U.S. Department of Energy Office of Science laboratory, operated under Contract DE-AC02-06CH11357 by UChicago Argonne, LLC.

References

1. Gao, F., Leach, R.K., Petzing, J, & Coupland, J.M. Surface measurement errors using commercial scanning white light interferometers. *Meas. Sci. Technol.* **19**, 015303 (2008).
2. Cheng, Y.-Y. & Wyant, J.C. Multiple-wavelength phase-shifting interferometry. *Appl. Opt.* **24**, 804-807 (1985).
3. Kino, G.S. & Chim, S.S.C. Mirau correlation microscope. *Appl. Opt.* **29**, 3775-3783 (1990).
4. Wyant, J.C. White light interferometry. *Proc. SPIE.* **4737**, 98-107 (2002).
5. Sakseev, D.A., Ershenko, E.M., Baryshev, S.V., Bobyl, A.V., & Agafonov, D.V. Deep microrelief measurement and stereo photography in scanning electron microscopy. *Tech. Phys.* **56**, 127-131 (2011).
6. Morris, R.J.H. & Dowsett, M.G. Ion yields and erosion rates for Si1-xGex (0≤x≤1) ultralow energy O2+ secondary ion mass spectrometry in the energy range of 0.25-1 keV. *J. Appl. Phys.* **105**, 114316 (2009).
7. O'Mahony, C., Hill, M., Brunet, M., Duane, R., & Mathewson, A. Characterization of micromechanical structures using white-light interferometry. *Meas. Sci. Technol.* **14**, 1807-1814 (2003).
8. Andersen, H.H. & Bay, H.L. Sputtering yield measurements. *Topics in Applied Physics Vol. 47: Sputtering by Particle Bombardment I.*, Behrisch, R., ed., Springer-Verlag, Berlin, Heidelberg, 145-218 (1981).
9. Wu, S.-M., van de Kruijs, R., Zoethout, E., & Bijkerk, F. Sputtering yields of Ru, Mo, and Si under low energy Ar+ bombardment. *J. Appl. Phys.* **106**, 054902 (2009).
10. Liu, X., Du, D., & Mourou, G. Laser ablation and micromachining with ultrashort laser pulses. *IEEE J. Quantum Electron.* **33**, 1706-1716 (1997).
11. Gattass, R.R. & Mazur, E. Femtosecond laser micromachining in transparent materials. *Nature Photonics* **2**, 219-225 (2008).
12. Russo, R.E., Mao, X., Gonzalez, J.J., & Mao, S.S. Femtosecond laser ablation ICP-MS. *J. Anal. At. Spectrom.* **17**, 1072-1075 (2002).
13. Brady, J.J., Judge, E.J., & Levis, R.J. Analysis of amphiphilic lipids and hydrophobic proteins using nonresonant femtosecond laser vaporization with electrospray post-ionization. *J. Am. Soc. Mass Spectrom.* **22**, 762-772 (2011).
14. Berry, J.I., Sun, S., Dou, Y., Wucher, A., & Winograd, N. Laser desorption and imaging of proteins from ice via UV femtosecond laser pulses. *Anal. Chem.* **75**, 5146-5151 (2003).
15. Coello, Y., Jones, A.D., Gunaratne, T.C., & Dantus, M. Atmospheric pressure femtosecond laser imaging mass spectrometry. *Anal. Chem.* **82**, 2753-2758 (2010).
16. Korte, F., Serbin, J., Koch, J., Egbert, A., Fallnich, C., Ostendorf, A., & Chichkov, B.N. Towards nanostructuring with femtosecond laser pulses. *Appl. Phys.* A **77**, 229-235 (2003).

17. Fu, Y., Bryan, N.K.A., Shing, O.N., & Wyan, H.N.P. Influence analysis of dwell time on focused ion beam micromachining in silicon. *Sensors and Actuators A.* **79**, 230-234 (2000).
18. Jiang, F., Li, J., Yan, L., Sun, J., & Zhang, S. Optimizing end-milling parameters for surface roughness under different cooling/lubrication conditions. *Int. J. Adv. Manuf. Technol.* **51**, 841-851 (2010).
19. Reiter, A.E., Mitterer, C., Figueiredo, M.R., & Franz, R. Abrasive and adhesive wear behavior of arc-evaporated Al1-xCrxN hard coatings. *Tribol. Lett.* **37**, 605-611 (2010).
20. Devillez, A., Lesko, S., & Mozer, W. Cutting tool crater wear measurement with white light interferometry. *Wear* **256**, 56-65 (2004).
21. Shekhawat, V.K., Laurent, M.P., Muehleman, C., & Wimmer, M.A. Surface topography of viable articular cartilage measured with scanning white light interferometry. *Osteoarthritis and Cartilage* **17**, 1197-1203 (2009).
22. Hershberger, J., Öztürk, O., Ajayi, O.O., Woodford, J.B., Erdemir, A., Erck, R.A., & Fenske, G.R. Evaluation of DLC coatings for spark-ignited, direct-injected fuel systems. *Surf. Coat. Technol.* **179**, 237-244 (2004).
23. Ajayi, O.O., Erck, R.A., Lorenzo-Martin, C., & Fenske, G.R. Frictional anisotropy under boundary lubrication: Effect of surface texture. *Wear.* **267**, 1214-1219 (2009).
24. Wittmaack, K. Analytical description of the sputtering yields of silicon bombarded with normally incident ions. *Phys. Rev. B.* **68**, 235211 (2003).
25. Zeuner, M., Neumann, H., Scholze, F., Flamm, D., Tartz, M., & Bigl, F. Characterization of a modular broad beam ion source. *Plasma Sources Sci. Technol.* **7**, 252-267 (1998).
26. Barna, A., Menyhard, M., Kotis, L., Kovacs, G.J., Radnoczi, G., Zalar, A., & Panjan, P. Unexpectedly high sputtering yield of carbon at grazing angle of incidence ion bombardment. *J. Appl. Phys.* **98**, 024901 (2005).
27. Weck, A., Crawford, T.H.R., Wilkinson, D.S., Haugen, H.K., & Preston, J.S. Laser drilling of high aspect ratio holes in copper with femtosecond, picosecond and nanosecond pulses. *Appl. Phys. A.* **90**, 537-543 (2008).
28. Roosendaal, H.E. Sputtering yields of single crystalline targets. *Topics in Applied Physics Vol. 47: Sputtering by Particle Bombardment I*., Behrisch, R., ed., Springer-Verlag, Berlin, Heidelberg, 219-256 (1981).
29. Seah, M.P. An accurate semi-empirical equation for sputtering yields II: For neon, argon and xenon ions. *Nucl. Instrum. Methods Phys. Res. B.* **229**, 348-358 (2005).
30. Seah, M.P., Clifford, C.A., Green, F.M., & Gilmore, I.S. An accurate semi-empirical equation for sputtering yields I: For argon ions. *Surf. Interface Anal.* **37**, 444-458 (2005).
31. Ziegler, J.F. SRIM: The Stopping and Range of Ions in Matter software, http://www.srim.org (2011).
32. Moller, W. & Eckstein, W. Tridyn - A TRIM simulation code including dynamic composition changes. *Nucl. Instrum. Methods Phys. Res. B.* **2**, 814-818 (1984).
33. Insepov, Z., Norem, J., & Veitzer, S. Atomistic self-sputtering mechanisms of *rf* breakdown in high-gradient linacs. *Nucl. Instrum. Methods Phys. Res. B.* **268**, 642-650 (2010).
34. Puech, L., Dubarry, C., Ravel, G., & de Vito, E. Modeling of iron oxide deposition by reactive ion beam sputtering. *J. Appl. Phys.* **107**, 054908 (2010).
35. Ho, S., Tamakoshi, T., Ikeda, M., Mikami, Y., & Suzuki, K. Net sputtering rate due to hot ions in a Ne-Xe discharge gas bombarding an MgO layer. *J. Appl. Phys.* **109**, 084908 (2011).
36. Nakles, M.R. Experimental and Modeling Studies of Low-Energy Ion Sputtering for Ion Thrusters. *Master of Science in Aerospace Engineering Thesis*, Virginia Polytechnic Institute and State University, 1-129 (2004).
37. Hada, M., Ninomiya, S., Seki, T., Aoki, T., & Matsuo, J. Using ellipsometry for the evaluation of surface damage and sputtering yield in organic films with irradiation of argon cluster ion beams. *Surf. Interface Anal.* **43**, 84-87 (2011).
38. Kozole, J., Wucher, A., & Winograd, N. Energy deposition during molecular depth profiling experiments with cluster ion beams. *Anal. Chem.* **80**, 5293-5301 (2008).
39. von der Linde, D., & Sokolowski-Tinten, K. The physical mechanisms of short-pulse laser ablation. *Appl. Surf. Sci.* **154-155**, 1-10 (2000).
40. Margetic, V., Bolshov, M., Stockhaus, A., Niemax, K., & Hergenroder, R. Depth profiling of multi-layer samples using femtosecond laser ablation. *J. Anal. At. Spectrom.* **16**, 616-621 (2001).
41. Cui, Y., Moore, J.F., Milasinovic, S., Liu, Y., Gordon, R.J., & Hanley, L. Depth profiling and imaging capabilities of an ultrashort pulse laser ablation time of flight mass spectrometer. *Rev. Sci. Instrum.* **83**, 093702 (2012).
42. Borowiec, A., MacKenzie, M., Weatherly, G.C., & Haugen, H.K. Femtosecond laser pulse ablation of GaAs and InP: Studies utilizing scanning and transmission electron microscopy. *Appl. Phys. A.* **77**, 411-417 (2003).
43. Harasaki, A., Schmit, J., & Wyant, J.C. Offset of coherent envelope position due to phase change on reflection. *Appl. Opt.* **40**, 2102-2106 (2001).
44. Luttge, A. & Arvidson, R.S. Reactions at surfaces: A new approach integrating interferometry and kinetic simulations. *J. Am. Ceram. Soc.* **93**, 3519-3530 (2010).
45. Conroy, M. & Mansfield, D. Scanning interferometry: Measuring microscale devices. *Nature Photonics.* **2**, 661-663 (2008).
46. Harasaki, A. & Wyant, J.C. Fringe modulation skewing effect in white-light vertical scanning interferometry. *Appl. Opt.* **39**, 2101-2106 (2000).
47. Roy, M., Schmit, J., & Hariharan, P. White-light interference microscopy: Minimization of spurious diffraction effects by geometric phase-shifting. *Opt. Express.* **17**, 4495-4499 (2009).

